Optics and Lasers in Engineering 101 (2018) 16–22

Contents lists available at ScienceDirect

Optics and Lasers in Engineering

journal homepage: www.elsevier.com/locate/optlaseng

# A robust multi-image phase retrieval

Cheng Guo [a], Cheng Shen [a], Jiubin Tan [a], Xuejing Bao [a], Shutian Liu [b], Zhengjun Liu [a,*]

[a] Department of Automatic Test and Control, Harbin Institute of Technology, Harbin 150001, China
[b] Department of physics, Harbin Institute of Technology, Harbin 150001, China

ARTICLE INFO

*Keywords:*
Phase retrieval
Diffraction

ABSTRACT

The phase evaluation is not perfect by using three kinds of existing multi-image phase retrieval methods. The amplitude-phase retrieval scheme is employed for initializing the input of the Multi-stage algorithm to obtain a robust result. The synthesized axial multi-image phase retrieval technique is able to be highly accurate convergent with continuous phase distribution of $[0, 2\pi]$ and random phase distribution of $[0, \pi]$, which is also demonstrated to have sharper edge for reconstructed phase map in experiment. This paper will provide a powerful and useful guidance for axial multi-image phase retrieval.



## 1. Introduction

Iterative phase retrieval has been a powerful tool to reconstruct the complex amplitude of sample by the back-and-forth beam propagation between the measuring plane and the sample plane with the addition of different constraints. To date, iterative phase retrieval technique has been successfully applied in encryption [1,2], electron microscopy [3], quantum imaging [4], super-resolution imaging [5]. As the origin of iterative phase retrieval algorithm, Gerchberg-Saxton (GS) algorithm [6] reconstructs the phase of sample with a pair of known amplitude distribution at the sample plane and the measuring plane. Its low convergence speed and much sensitivity to the initial value, however, restrict its application. Moreover, another limitation of GS algorithm lies on that the amplitude distribution of sample has to be determined, which usually imposes more complexity in experimental setup. Thus, based on the origin, hybrid input output (HIO) algorithm [7] was brought up by using the support constraint to increase the convergence speed. In spite of higher convergence speed and high precision, both algorithms require that the support constraint should be tight.

To overcome these limitations, multi-image phase retrieval algorithms have been proposed [8–18] afterwards. They introduce variable optical system parameters to generate multiple measurements and get rid of the prior knowledge of amplitude distribution at the sample plane. The methodology can be divided into two categories: lateral and axial scanning strategies. As a lateral scanning technique, the ptychographic iterative engine (PIE) algorithm [8] shifts an aperture or a pinhole to create a series of overlapped diffraction patterns at the measuring plane. Its demanding shifting operation slows down the reconstruction and leads to a long acquisition time, which is then improved by LED array microscope [9], parallel calculation [10], and modulation imaging with a measured loose support [11]. Recently, these lateral scanning methods, such as single-shot pychography [12] and Fourier pychographic microscopy [5], have made lots of achievements theoretically and experimentally. For axial scanning, the single-beam, multiple-intensity reconstruction technique (SBMIR) algorithm [13] and the multi-stage algorithm [14] both sequentially record diffraction and then process them serially in the iterative update. By contrast, the amplitude-phase retrieval (APR) algorithm [15] deals with the measured diffraction patterns in a parallel way and averages the estimations in the real space. It has been demonstrated by experiment that these axial scanning algorithms can be realized by using focus tunable lens [16], multiple wavelengths [17], and multiple measuring distances [18].

Currently, all researches about these axial methods pay more attention on retrieving the object amplitude than the phase. But phase usually reflects much intrinsic information on the sample, for example, the thickness of transparent biological specimens. Also, the discussion of these methods does not cover the application range where the object size varies. Due to the two reasons, this paper investigates the performance of three axial multi-image phase retrieval algorithms, including SBMIR, Multi-stage and APR algorithm, under two typical object phase distributions. Then, we discover their respective disadvantages. To tackle the issue, we propose a new hybrid algorithm, which achieves robust phase reconstruction while keeping a high-precision amplitude retrieval and significantly reduces sensibility to the initialization. Also, we define the dynamic range where these axial methods can effectively work, which distinguishes them from the lateral scanning techniques. Thus, it will be an instructive guideline for applying these popular algorithms. At length, the performance of our hybrid approach is also demonstrated in experiment.

* Corresponding author.
*E-mail address:* zjliu@hit.edu.cn (Z. Liu).

http://dx.doi.org/10.1016/j.optlaseng.2017.09.014
Received 30 March 2017; Received in revised form 27 July 2017; Accepted 13 September 2017
0143-8166/

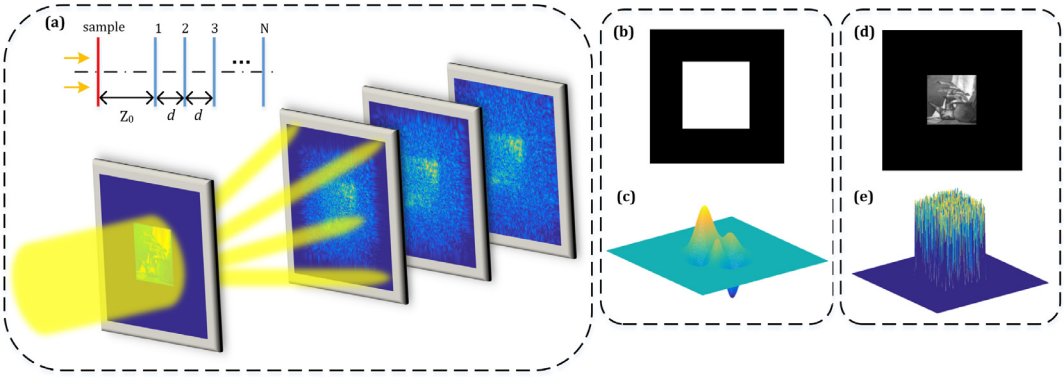


**Fig. 1.** Schematic diagram of axial multi-image phase retrieval experiment (a) and tested samples for simulation: the multiplication of (b) and (c) forms an ideal complex amplitude function with a continuous phase; (d) and (e) forms one with a random phase. Both of them are rasterized in 256 × 256 pixels.

## 2. Reconstructed performance analysis

Before the further analysis, the optical system parameters need to be declared. The total of intensity measurements N is 8. Here the angular spectrum analysis method is utilized to depict the free-space propagation in Fig. 1(a). To satisfy the sampling theorem in simulation, the pixel number of image M × M, the physical side length L, the working wavelength $\lambda$ and the diffraction distance Z should follow [19]

$$Z^2 \geq \frac{L^4}{M^2\lambda^2} - L^2. \tag{1}$$

Besides, it can be easily proved that once the first diffraction distance $Z_0$ meets the sampling condition, the sequential distances $Z = Z_0 + (n-1)d$, $1 \leq n \leq N$ comply with it as well.

Fig. 1(c) and (e) are two typical sample phase distributions, namely the continuous one and the random one. The former denotes the condition that the wave front gives a global smooth change and there are no singular points in the 2-D distribution. By contrast, the latter is generated from the normal Gaussian distribution, representing the condition with manifold jumps. Combined with a square pupil in Fig. 1(b) and a still object sketch picture in Fig. 1(d) [20] as the amplitude function separately, they form a pair of tested complex amplitude functions, which are taken as the ground truth for the following simulations.

Generally, the mean square error (MSE) between the reconstructed and true amplitude distribution is adopted as an indicator of recovery accuracy. In this paper, we utilize the modified version of this metric to clarify the retrieved quality for amplitude and it is defined as

$$\mathrm{LMSE} = \log_{10}\left(\frac{1}{M \times N}\sum_{\forall m,n} \left||A_{est}| - |A_0|\right|^2\right), \tag{2}$$

where $A_{est}$ and $A_0$ denote the reconstructed amplitude and the object amplitude respectively. For the phase, we bring standard deviation for phase convergence criterion like as [13]

$$\mathrm{LSTD} = \log_{10}\left[\mathrm{std}\left(\varphi_{est} - \varphi_0\right)\right], \tag{3}$$

where the symbol "std" denotes the standard deviation between the estimated phase $\varphi_{est}$ and the true phase $\varphi_0$.

When the continuous phase ranges from $-\pi$ to $\pi$ and the random phase from 0 to $\pi$, the LSTDs of these three axial algorithms are pictured in Fig. 2 as the intensity measurements are taken at different positions in the diffraction field of object. To denote the displacement, the first diffraction distance $Z_0$ increases from 15 mm to 110 mm with an interval of 5 mm. The distance $d$ between two consecutive measuring planes follows the same value variation as $Z_0$ does. The working wavelength is 632.8 nm. The initialization of these three methods is set as a zero matrix and the iterative procedure is executed until 1000 times in all simulations. With these assumptions, the recovery performance of whole diffraction filed is able to be built in Fig. 2. Especially, each pair of ($Z_0$, $d$) represents one of reconstructed results in the diffraction field.

As is shown in Fig. 2 (a)–(c), three axial algorithms behave differently for the recovery of object with a continuous phase. Two serial computing algorithms, SBMIR and Multi-stage, can obtain an excellent phase reconstruction wherever the measurements are in the diffraction field. However, the retrieved result from APR, the parallel multi-image algorithm, has a high LSTD from the ground truth overall, and even appears a failure at some peculiar measurement conditions.

It is the converse for the random phase condition. Almost all measurements from the whole diffractive field guarantee an accurate phase reconstruction for APR, whose LSTD keeps around −20 orders of magnitude in Fig. 2(e). Nevertheless, the error distributions from SBMIR algorithm and Multi-stage algorithm are quite wavy and fluctuate heavily at some particular pairs ($Z_0$, $d$) values shown in Fig. 2(d) and (f). This means that these two serial calculation strategies are sensitive to the position of measuring planes in the diffraction field. Once $Z_0$ is chosen improperly, they will converge to a wrong solution.

To conclude, neither of the serial and parallel multi-image algorithms are able to have stable excellent performance to retrieve different forms of phase. Usually, phase information reveals the variation of sample thickness or refractivity. Continuous phase distribution represents a low gradient variation of the index while random phase distribution belongs a high one. Considering that the observed sample is complicated in reality, it is nearly impossible to predict the phase form ahead. Therefore, both serial and parallel calculating methods could be impotent. Also, the sample phase distribution may behave a mixture of the continuous and random ones. An ambidextrous algorithm is needed to tackle the phase issue.

## 3. Hybrid approach

Here, we put forward a hybrid scheme: (a) using the first guess of APR algorithm as the initialization; (b) carrying on the iteration with Multi-stage algorithm. Its flowchart is illustrated in Fig. 3. The symbol $I_N$ denotes the measured intensity. G is the propagation operator, which represents the diffraction computation in free space. The superscript '$\alpha$' and '-$\alpha$' denote forth and back propagation separately.

In order to evaluate the convergence stability of three existing algorithms and the hybrid approach for the measurements from the whole diffraction field, we define a parameter, GPRQ (global phase retrieval quality). $P_{Z_0,d}$ represents the reconstructed phase distribution under the first diffraction distance $Z_0$ and the interval $d$. The variables $(P^1_{Z_0,d}, P^2_{Z_0,d}, \ldots, P^{N_1+N_2}_{Z_0,d})$ denote overall reconstructed results for whole diffraction filed. In addition, we emphasize on whether or not phase retrieval is sufficiently convergent, in this case, $\mathrm{LSTD}(P_{Z_0,d})$must be a negative parameter here. If its LSTD satisfies

$$LSTD\left(P_{Z_0,d}\right) > \frac{1}{\beta}\min\left[LSTD\left(P^1_{Z_0,d}, P^2_{Z_0,d}, \ldots, P^{N_1+N_2}_{Z_0,d}\right)\right], \tag{3a}$$

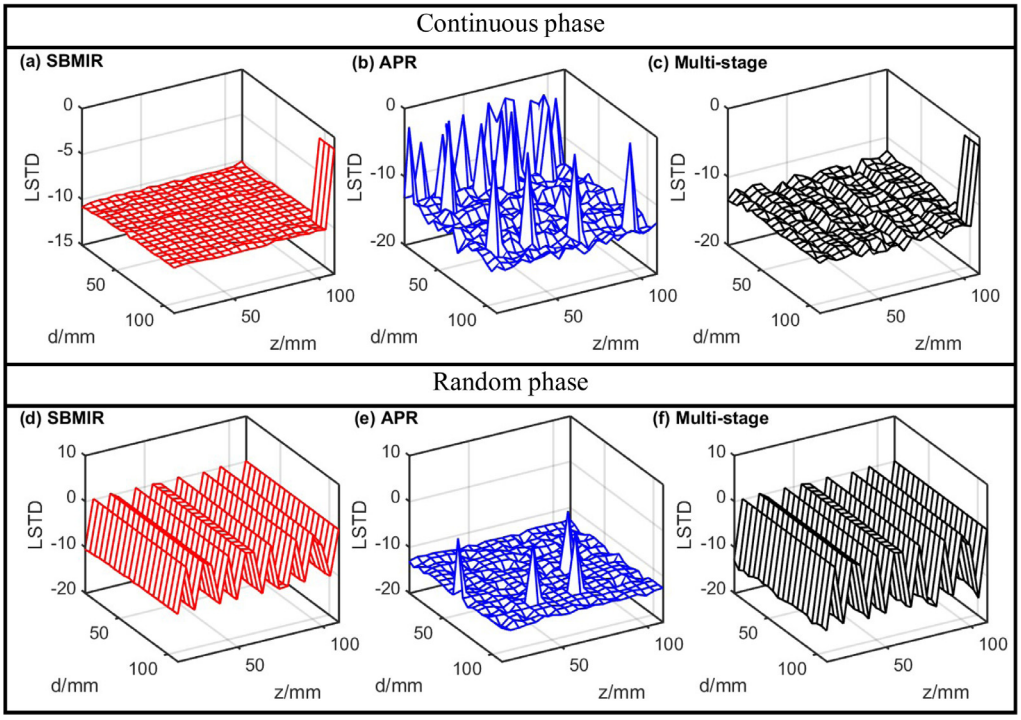


**Fig. 2.** LSTD of continuous and random phase retrieval from three axial multi-image algorithms when the measurements are taken at different places in the diffractive field.

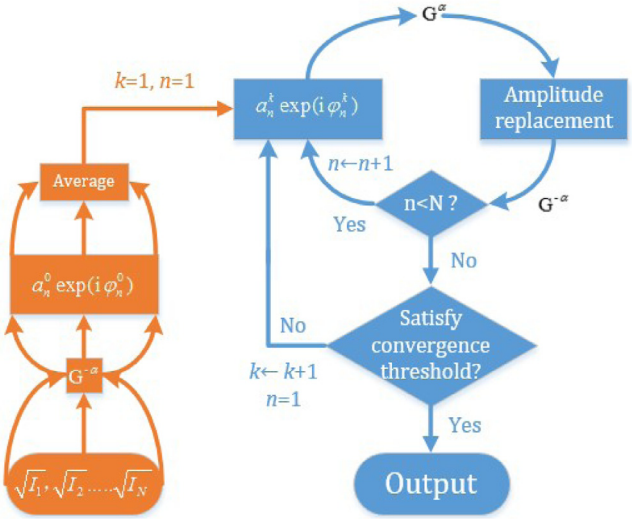


**Fig. 3.** Flowchart of the hybrid approach. The orange part is a parallel calculation of APR algorithm to generate an initialization for the blue part, Multi-stage algorithm. (For interpretation of the references to color in this figure legend, the reader is referred to the web version of this article)

compared to the minimum of all LSTDs under different $Z_0$ and $d$, it will be counted into $N_1$ as bad position pairs. These bad places comprise the slow-convergent or even non-convergent region in the whole diffraction field, namely 'dead zone'. The number of the other places is $N_2$. As a threshold factor, $\beta$ is 2 here but it is adjustable for different situations and will not affect the final analysis. Thus, we have

$$\mathrm{GPRQ} = \frac{N_2}{N_1 + N_2}, \tag{4}$$

as an indicator of convergence stability for phase retrieval. The larger GPRQ is, the better the algorithm performs.

Fig. 4 illustrates the global phase retrieval quality of four algorithms under two types of phase distributions. As phase range of object changes, the GPRQ curves are done while K ranges from 0 to 40. In Fig. 4, each GPRQ under one K denotes convergence stability of whole diffraction field, which is derived from the computation of many pairs of ($Z_0$, $d$) like as Fig. 2. Hence the GPRQ curves in Fig. 4 are time-consuming and data-heavy so that the assessment of convergence stability is reliable. For continuous phase, the phase range is selected as [-K$\pi$/20, K$\pi$/20], $0 \le K \le 40$, K∈Z. For random phase, its range is chosen as [0, K$\pi$/20], $0 \le K \le 40$, K∈Z. Especially, the reason why the tested range of random phase is not fixed as like the range of continuous phase is that the random phase with [-K$\pi$, K$\pi$], K∈Z, is entirely non-convergent.

Overall, GPRQ of these axial multi-image algorithms decreases as the range of object phase increases. As far as the continuous phase is concerned in Fig. 4(a), three old algorithms can achieve the perfect recovery only in the range of [$-0.8\pi$, $0.8\pi$]. However, the hybrid scheme holds the high performance for the whole phase range. In Fig. 4(b), it indicates that the hybrid scheme can work as well as APR algorithm, prior to the other old algorithms. Its stable convergent range is parameterized as K = 20, namely [0, $\pi$]. In addition, the maximum of gradient (MG) of object phase surface for every K is used as a quantitative metric for these two types phase modalities, which are depicted in the bottom left of Fig. 4(a) and (b). Obviously, continuous phase denotes a target with a low gradient variation. On the contrary, random phase aims at a high one. As we expect, hybrid approach holds stable convergence in both continuous and random phase, which actually improves the stability of axial multi-image phase retrieval.

On the basis of Multi-stage algorithm, our hybrid approach replaces its initial guess with one iteration of APR algorithm. Hence the comparison between hybrid approach and Mutli-stage algorithm with different initial guesses is essential to be given out. After feeding initialization value of 0, 1 and random data, the reconstructed image's standard deviations of the continuous phase are listed in Table 1. It is noted that our hybrid approach tremendously raises the insensibility to the initialization. Even if facing with dead points, hybrid approach is still able to achieve high-accuracy reconstruction.

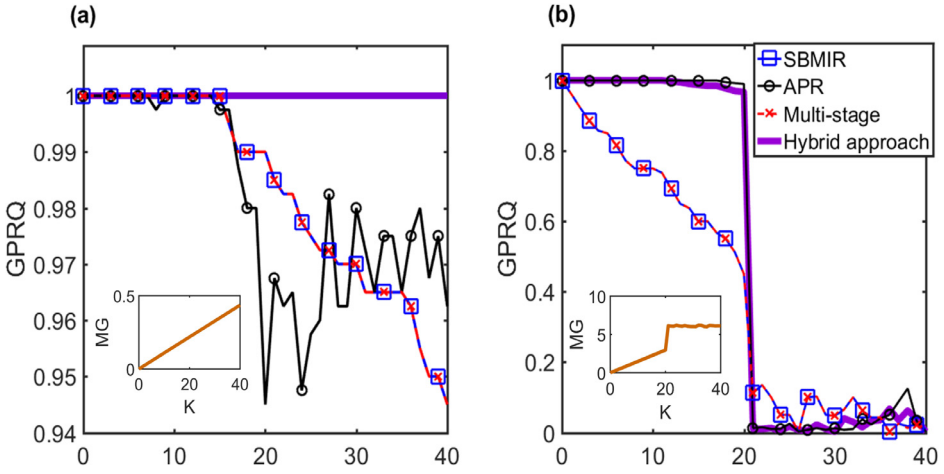


**Fig. 4.** Global phase retrieval quality (GPRQ) of three axial multi-image phase retrieval and hybrid approach for continuous and random phase. (a) Continuous phase with the range of [-K$\pi$/20, K$\pi$/20], $0 \le K \le 40$, K∈Z; (b) Random phase with the range of [0, K$\pi$/20], $0 \le K \le 40$, K∈Z.

**Table 1**
Standard deviation of reconstructed results under different initial values.

| Algorithm | ($Z_0$, $d$) unit: mm | 0 | 1 | Random data1 | Random data2 |
|---|---|---|---|---|---|
| Multi-satge | (20, 80) | 0.08 | 0.08 | 0.08 | 0.08 |
| | (20, 90) | 0.11 | 0.11 | 0.11 | 0.11 |
| | (110, 30) | 0.09 | 0.09 | 0.09 | 0.09 |
| | (110, 40) | 0.07 | 0.07 | 0.07 | 0.07 |
| Hybrid approach | (20, 80) | $5.1\times10^{-14}$ | $5.1\times10^{-14}$ | $5.1\times10^{-14}$ | $5.1\times10^{-14}$ |
| | (20, 90) | $5.1\times10^{-14}$ | $5.1\times10^{-14}$ | $5.1\times10^{-14}$ | $5.1\times10^{-14}$ |
| | (110, 30) | $4.3\times10^{-15}$ | $4.3\times10^{-15}$ | $4.3\times10^{-15}$ | $4.3\times10^{-15}$ |
| | (110, 40) | $1.6\times10^{-13}$ | $1.6\times10^{-13}$ | $1.6\times10^{-13}$ | $1.6\times10^{-13}$ |

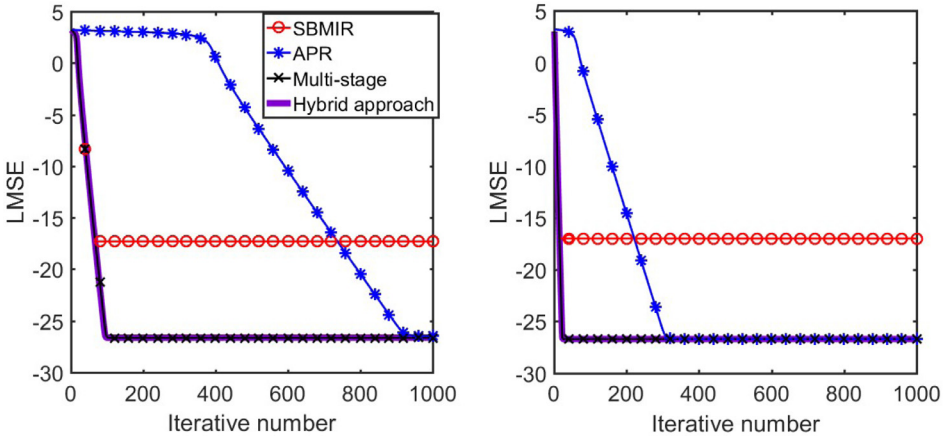


**Fig. 5.** Amplitude retrieval convergence curve of four algorithms. (a) four measured intensity patterns as the input; (b) eight measured intensity patterns as the input.

Except the advantages in phase retrieval, we also test the amplitude retrieval ability of the hybrid approach. As is shown in Fig. 5, its convergence curve overlaps the Multi-stage one. Also, it converges to the smallest LMSE, namely a more accurate result. For convergence speed, SBMIR algorithm holds the first place, multi-stage method comes second and APR method gets the last. Therefore, the hybrid approach inherits the merits from both serial and parallel methods.

The hybrid method can combine resverel images into an optical diffraction process. It has potential application in color image encryption or multiple image encryption [1]. The phase retrieval algorithm will obtain a more accurate distribution of phase mask in optical system hiding serevel secret image. At the same time, the quality of expected encrypted image will be enhanced due to the small error of phase filters designed with the hybrid approach.

## 4. Dynamic range

Here the dynamic range is investigated where these axial methods are effective. In simulation, $Z_0$ is set as 100 mm and $d$ equals to 20 mm, with eight measurements. The lengths of object image variates from 2 to 8 mm, where some propagation distances cause under-sampling.

In Fig. 6(a), the oversampling range $L \le 3$ mm, out of which sampling condition belongs to undersampling. We perform three axial methods and hybrid approach with different sampling length under 1000 and 3000 iterations. Accordingly, the LSTDs of reconstructed images go up with the increase of sampling length. Note that even using large numbers of iterations are incapable of successful recovery when the sampling condition Eq. (1) is not satisfied.

As is opposite to Fig. 6(a), Fig. 6(b) shows the case where the sampling condition is strictly met for each diffraction distance, which is im-

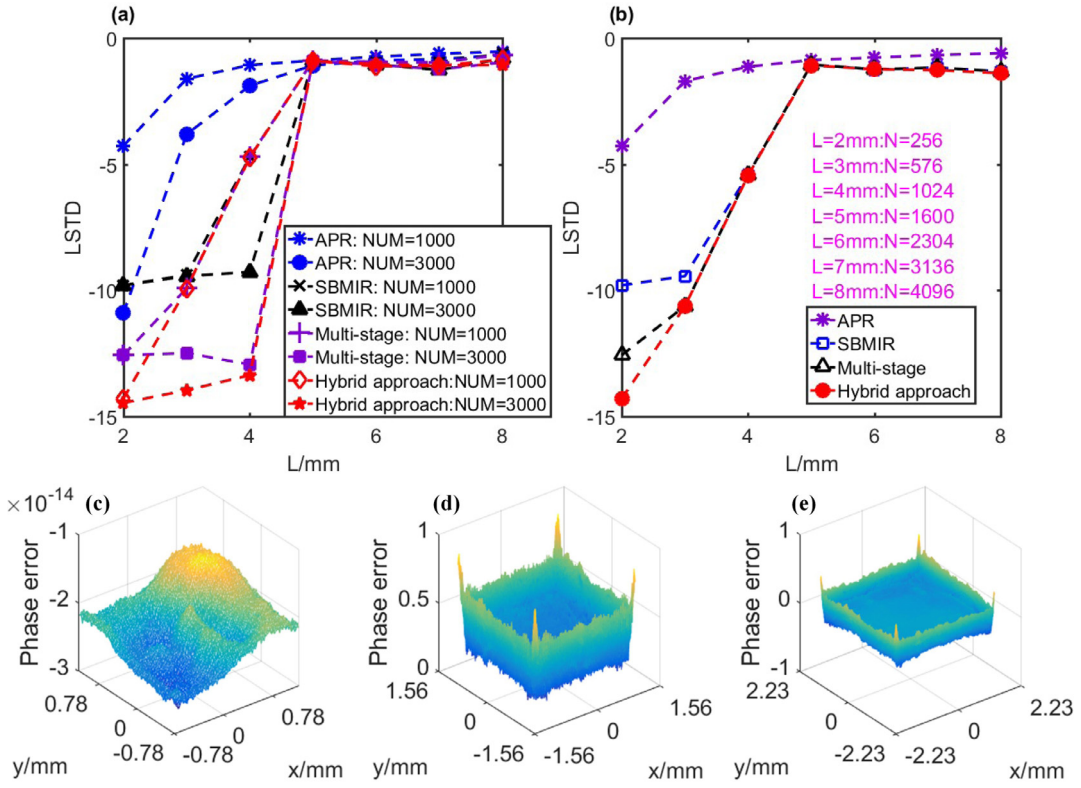


**Fig. 6.** Reconstruction errors of four axial multi-image algorithms when the continuous phase is the input: (a) shows LSTD as the function of the object side length L and the iteration number NUM, in which the sample condition is not strictly met. (b) shows the case satisfying the sample condition totally with NUM = 1000. (c-e) are the reconstruction error from hybrid approach respectively, with L = 2 mm, L = 5 mm and L = 7 mm in (b), respectively.

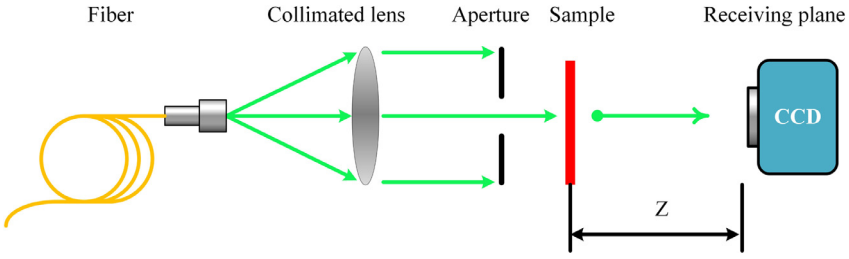


**Fig. 7.** The schematic of experiment.

plented by using enough sampling pixels for each side length. The sampling pixels corresponding to each sampling length are listed by pink font inside Fig. 6(b). It is surprising that these axial multi-image phase retrieval algorithms are still unable to get the satisfactory reconstruction while L is beyond 5 mm. In other words, they have a limited application range related to the physical size of object. The increase of object size will end up with a failure of phase retrieval. For example, Fig. 6(c)–(e) display the error of recovered and true phase ($\varphi_{est} - \varphi_0$) for hybrid approach when L = 2 mm, 5 mm and 7 mm. L = 2 mm, strictly satisifying Eq. (1), achieves phase recovery with magnitude of $10^{-14}$ shown in Fig 6(c), which is successful to retrieve a full phase surface of object. The rest have distortions to some extent, compared to Fig. 6(c). Therefore, we need to carefully pick up the suitable scheme for the observed object according to its physical size.

## 5. Experiment

Here the experimental schematic is shown in Fig. 7. A fiber laser (532 nm) incidents on a collimated lens to form a plane wave illumination. This plane beam passes through aperture to illuminate sample and the corresponding diffraction patterns ($Z = Z_0 + (n-1)d$, $1 \le n \le N$) are received by CCD camera (3.1 μm, Point Gray). Here the movement along z axis is done by a precision linear stage (M-403, resolution 0.012 μm, Physik Instrumente Inc.).

In experiment, we employ a cross-shaped arrow as the sample and its reconstructed results are displayed in Fig. 8. To obersve the performance of phase retrieval, CCD camera is sequentially placed far away from the sample ($Z_0 = 240$ mm, d = 2 mm, N = 11). The sampling length is chosen as 4.34 mm (1400 × 1400 pixels). After 20 iterations, the reconstructed results are given in Fig. 8. For amplitude, it is difficult to tell the difference among them. On the contrary, the improvement of hybird approach is manifested by means of recovered phase. Compared to APR, SBMIR and Multi-stage methods, the reconstucted phase map of hybrid approach owns sharpest edge for chosen target, which demonstrates that hybrid approach has excellent convergence quality.

Another target, a part of USAF1951 resolution chart (R3L3S1N, Thorlabs), is utilized as sample and its retrieved results are shown in Fig. 9. Similar to Fig. 8, the enhancement of hybird approach is not discerned from reconstructed amplitude in Fig. 9(a). But its structure is easy to be recognized for retrieved phase map. In other words, phase contrast is strengthened on the edge of target for hybrid approach. As we capture data along the direction of black arrow, the slicing outlines

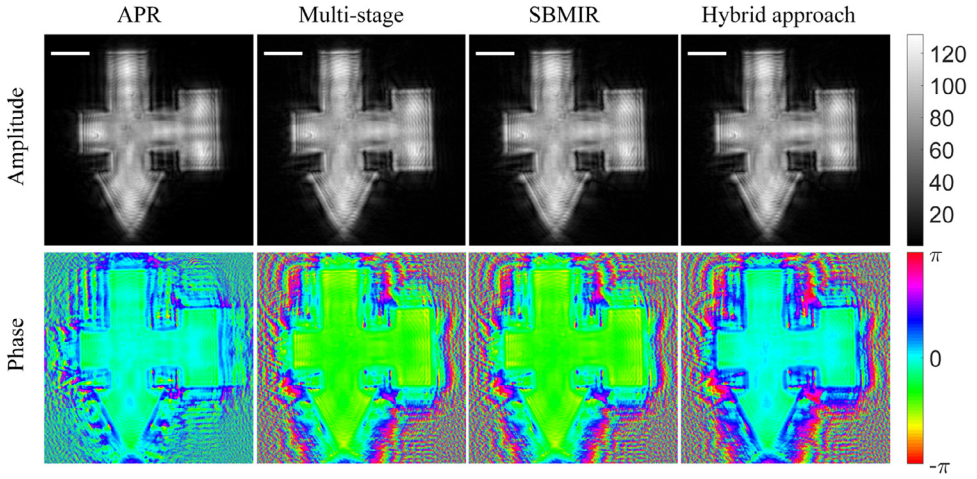


**Fig. 8.** The reconstructed amplitude and phase of cross-shaped arrow target for APR, SBMIR, Multi-stage and hybrid approach algorithm. The white bars correspond to 800 μm.

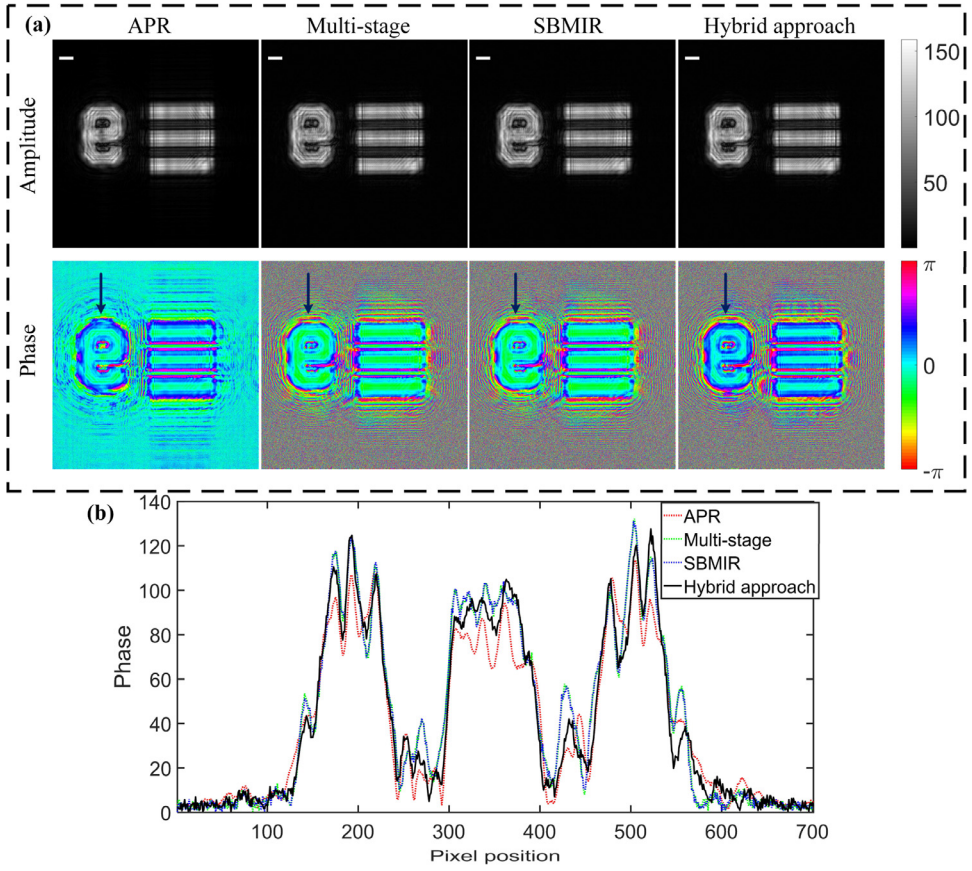


**Fig. 9.** The reconstructed results of resolution chart for four algorithms. (a) reconstructed amplitudes and phases; (b) line plots of phase along black arrow. The white bars correspond to 300 μm.

of four recovered phase are shown in Fig. 9(b). It is noted from Fig. 9(b) that hybrid approach holds peak value similar to Multi-stage algorithm and valley value similar to APR algorithm, which proves that hybrid approach combine APR and Multi-stage method well. As we expect, this combination enhances the phase contrast for axial multi-image phase retrieval.

## 6. Conclusion

To sum up, this paper studies the performance of SBMIR, Multi-stage and APR algorithms under two typical object phase distributions and point out their weakness. We put up a hybrid algorithm to tackle the phase problem. The new hybrid algorithm can not only recover different forms of phase, but also obtains a high-precision amplitude retrieval and significantly reduces sensibility to the initialization. Also, the application range limited by the physical size of object is given for these axial methods. The knowledge is very instructive when applying the iterative schemes. At last, these three algorithms and hybrid approach are performed in experiment, which demonstrates that our hybrid approach enhances the contrast of reconstructed phase. Multiple distance measurements, as a lensless imaging technique, is able to facilitate a compact and simple imaging implementation. With the plug-in of our

hybrid approach, the robustness and stability of mutli-distance phase retrieval is actually improved, which could be a useful and effective tool for phase imaging or super resolution techqiue.

## Acknowledgments

This work was supported by the National Natural Science Foundation of China (Nos. 61377016, 61575055 and 61575053), the Program for New Century Excellent Talents in University (No. NCET-12-0148), the China Postdoctoral Science Foundation (Nos. 2013M540278 and 2015T80340), the Fundamental Research Funds for the Central Universities (No. HIT.BRETIII.201406), the Scientific Research Foundation for the Returned Overseas Chinese Scholars, State Education Ministry, China.

## References

[1] Liu Z, Guo C, Tan J, Liu W, Wu J, Wu Q, et al. Securing color image by using phase-only encoding in Fresnel domains. Opt Lasers Eng 2015;68:87–92.
[2] Alfalou A, Brosseau C. Chapter two - recent advances in optical image processing. Prog Opt 2015;60:119–262.
[3] Humphry MJ, Kraus B, Hurst AC, Maiden AM, Rodenburg JM. Ptychographic electron microscopy using high-angle dark-field scattering for sub-nanometre resolution imaging. Nat Commun 2012;3:730.
[4] Liberman L, Israel Y, Poem E, Silberberg Y. Quantum enhanced phase retrieval. Optica 2016;3 193–9.
[5] Zheng G, Horstmeyer R, Yang C. Wide-field, high-resolution Fourier ptychographic microscopy. Nat Photon 2013;7 739–45.
[6] Gerchberg RW, Saxton WO. A practical algorithm for the determination of phase from image and diffraction plane pictures. Optik 1972;35 237–46.
[7] Fienup JR. Phase retrieval algorithms: a comparison. Appl Opt 1982;21 2758–69.
[8] Rodenburg JM, Faulkner HML. A phase retrieval algorithm for shifting illumination. Appl Phys Lett 2004;85 4795–7.
[9] Tian L, Waller L. 3D intensity and phase imaging from light field measurements in an LED array microscope. Optica 2015;2 104–11.
[10] Nashed YSG, Vine DJ, Peterka T, Deng J, Ross R, Jacobsen C. Parallel ptychographic reconstruction. Opt Express 2014;22 32082–97.
[11] Zhang F, Chen B, Morrison GR, Vila-Comamala J, Guizar-Sicairos M, Robinson IK. Phase retrieval by coherent modulation imaging. Nat Commun 2016;7:13367.
[12] Sidorenko P, Cohen O. Single-shot ptychography. Opitca 2016;3:9–14.
[13] Pedrini G, Osten W, Zhang Y. Wave-front reconstruction from a sequence of Interferograms recorded at different planes. Opt Lett 2005;30 833–5.
[14] Rodrigo JA, Duadi H, Alieva T, Zalevsky Z. Multi-stage phase retrieval algorithm based upon the gyrator transform. Opt Express 2010;18 1510–20.
[15] Liu Z, Guo C, Tan J, Wu Q, Pan L, Liu S. Iterative phase-amplitude retrieval with multiple intensity images at output plane of gyrator transforms. J Opt 2015;17:025701.
[16] Mosso F, Peters E, Perez DG. Complex wavefront reconstruction from multiple-image planes produced by a focus tunable lens. Opt Lett 2015;40 4623–6.
[17] Bao P, Zhang F, Pedrini G, Osten W. Phase retrieval using multiple illumination wavelengths. Opt Lett 2008;33 309–11.
[18] Shen C, Tan J, Wei C, Liu Z. Coherent diffraction imaging by moving a lens. Opt Express 2016;24 16520–9.
[19] Goodman J. Introduction to Fourier optics. Greenwood Village: Roberts & Co; 2005.
[20] Gonzalez RC, Woods RE. Digital image processing. New Jersey: Pearson/Prentice Hall; 2008.